Fabrication of Zinc Incorporated Magnetic Iron Oxide Nanoparticles for Photocatalytic Degradation of Methylene Blue

Emmanuel, Nleonu Chile [1+•]
Department of Chemistry, Federal Polytechnic Nekede, Owerri, Imo State, NIGERIA.

Ifeoma, Okeke Pamela
Department of Basic Sciences, Alvan Ikoku Federal College of Education, Owerri, Imo State, NIGERIA.

Chijioke Onyemenonu, Christopher
Department of Chemistry, Federal Polytechnic Nekede, Owerri, Imo State, NIGERIA.

Gaya, Umar Ibrahim
Department of Pure and Industrial Chemistry, Bayero University Kano, Kano State, NIGERIA.

Nazir, Muhammad Altaf
Institute of Chemistry, The Islamia University of Bahawalpur, Bahawalpur, PAKISTAN.

Ahmad Shah, Syed Shoaib
Key Laboratory of Luminescence Analysis and Molecular Sensing, Ministry of Education, School of Materials and Energy, Southwest University, Chongqing, P.R. CHINA.

ABSTRACT: *The fabrication of sustainable and efficient metal oxide-based semiconductor materials for effective degradation of environmental pollutants and other applications are currently attracting major interest from researchers. For this reason, magnetic iron oxide (Fe_3O_4) and zinc incorporated magnetic iron oxide ($Zn@Fe_3O_4$) nanoparticles were successfully synthesized by a co-precipitation method and tested for their physical properties and also as a photocatalysts for the degradation of toxic dye from the environment. The photocatalyst were analyzed by the use of Scanning Electron Microscopy (SEM), X-Ray Diffraction (XRD) and Ultra-Violet Visible spectrophotometer to evaluate their morphology, crystallinity and band gap properties, respectively. The photocatalytic degradation performance of synthesized nano-Fe_3O_4 and $Zn@Fe_3O_4$ was studied for their degradation efficiency on Methylene Blue (MB) dye. The photocatalytic activity of nano-Fe_3O_4 was affected by doping with Zn ion. The highest methylene blue degradation (83.80 % and 70.50 %) for nano-Fe_3O_4 and $Zn@Fe_3O_4$ were obtained at 0.5 g dose. The XRD and SEM results approved the existence of nano-Fe_3O_4 and $Zn@Fe_3O_4$, and also*

1 To whom correspondence should be addressed.
+E-mail: enleonu@yahoo.com, cnleonu@fpno.edu.ng
1021-9986/2023/11/3590-3600 11/$/6.01
● *Another Address: Materials and Electrochemical Research Unit (MERU), Department of Chemistry, Federal Polytechnic Nekede, Owerri, Imo State, NIGERIA.*

highlighted the successful entrance of zinc ion onto nano-Fe_3O_4. The introduction of zinc dopant into Fe_3O_4 lattices increases the band gap from 2.77 eV to 2.80 eV. The study of electronic structure of methylene blue was examined through quantum chemical calculations using Density Functional Theory (DFT) method in order to give an insight on the nature of MB interaction with synthesized photocatalyst. The DFT results revealed that the nitrogen atom of the MB molecule is the favorite sites of interaction with the metal oxide surface. Furthermore, the experimental findings showed that magnetic iron oxide demonstrated a good photocatalyst in degradation of methylene blue as compared to the zinc doped magnetic iron oxide particle.

KEYWORDS: *Photocatalysis, Computational modeling, Metal oxide, Metal dopant, Methylene blue.*

INTRODUCTION

Industrial effluents from various industries constitute the major cause of contamination of natural waters, specifically in developing or underdeveloped countries [1-3]. The pollution of textile wastewaters is especially caused by dyes and has caused serious environmental problems [4]. These wastewaters consist of high concentration of colored, non-biodegradable, organic dyes, having the ability to accumulate and persist in the environment for a prolonged time [5, 6]. They are generally carcinogenic and toxic to aquatic and human life [2, 7]. Methylene Blue (MB) dye with chemical formula $C_{16}H_{18}N_3ClS$ is a basic synthetic dye used in the leather, textile, paper printing industries and medical field. Because of its stability, it can exist in the environment for a long period of time and cause detrimental effects on aquatic plants and animals [8, 9]. Waste waters containing dyestuff are extremely difficult to treat due to their synthetic nature and complex aromatic structure [10]. Recent researches have paid attention in overcoming these problems by employing various decolourization and degradation methods. Various strategies have been employed for the elimination of various contaminants in polluted wastewaters such as, biodegradation, coagulation, adsorption methods [11,12].

Among several approaches, advanced oxidation method based on photocatalytic oxidation seems a favourable approach due to its ability to cause mineralization of the pollutants. It is cost-effective, easy operation-wise, less toxic, and highly efficient [6,13]. Photocatalysis usually employs a semiconductor photocatalyst and light for the treatment of dye polluted wastewater [5,6]. Metal oxides of transition elements are among the attractive materials for industrial application because of their high stability under ultraviolet light, low cost, high resistance to corrosion and their relative abundance [3]. Magnetic iron oxide (Fe_3O_4) nanoparticles have received great attention because of their eco-friendly, low cost, non-toxicity, remarkable magnetic, catalytic, electrical, optical, and high stability properties which enhance its applications in diverse areas [14]. The benefits of working with Fe_3O_4 nanoparticles include, easy of separation from the reaction medium due to its high magnetic power, reusability and high light absorption power [15]. The energy gap (E_g) between the valence band of Fe(4s) and O(2p) in Fe_3O_4 is 2.1 eV (309-206 nm) [16]. Notwithstanding the previous reports of poor performance of this semiconductor composite with TiO_2 due to recombination, metal dopants may enhance its photocatalytic efficiency [5,17]. Metal doping may lead to the creation of intra-band levels that narrows the band gap and improve photocatalyst efficiency by influencing the light absorption, photo-reactivity and morphology of semiconductor photocatalyst [10]. Doping with Zinc (II) ion is thought to have a great potential because of the closeness of the ionic radius of Zn^{2+} (0.74 Å) to that of Fe^{3+} (0.76 Å), as this is expected to reduce the band gap energy required for excitation and enhances Photoactivity [16].

A comprehensive study from literature has shown the fact that doped metal oxide enhances their properties in order to employ them in photocatalysis and photodegradation [18]. According to the best of our knowledge, no studies have been reported on the incorporation of zinc ion into Fe_3O_4 in the photocatalytic degradation of MB from aqueous environments. The novelty of this study is mainly focused on the synthesis; characterization and application

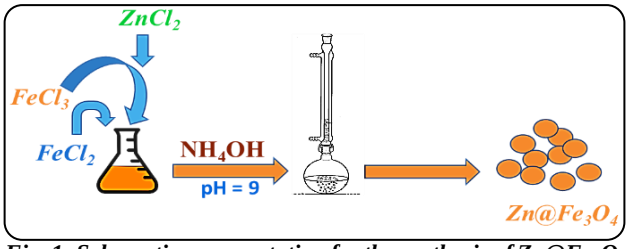

Fig. 1: Schematic representation for the synthesis of Zn@Fe₃O₄

of Fe_3O_4 and $Zn@Fe_3O_4$ as a photocatalyst for the degradation of MB from aqueous solution that previously have not been described. In this study, doped and undoped photocatalysts (Fe_3O_4 and $Zn@Fe_3O_4$) were synthesized by a coprecipitation method and analyzed using X-Ray Diffraction (XRD), UV-Visible spectroscopy and Scanning Electron Microscopy (SEM). The photocatalytic degradation efficiency of synthesized Fe_3O_4 and $ZnFe_3O_4$ were examined based on the decolorization of methylene blue in aqueous medium supported by theoretical studies using DFT density functional theory.

EXPERIMENTAL SECTION

Materials

Analytical grade reagents were used as received, without further purification in the present study. Iron (II) chloride tetra-hydrate ($FeCl_2.4H_2O$, 98 %), iron (III) chloride hexa-hydrate ($FeCl_3.6H_2O$, 98 %), zinc chloride ($ZnCl_2$, 99 %), ammonium hydroxide (NH_4OH, 98 %), sodium hydroxide (NaOH, 98 %) and methylene blue (98 %) were products of Loba Chemie PVT. Ltd, India. Deionized water was used as a solvent in all the experimental studies.

Synthesis of Fe_3O_4

Chemical co-precipitation method was used for Fe_3O_4 synthesis using ferric chloride, ferrous chloride and ammonium hydroxide [19]. Ferric solution was prepared by adding 17.59 g $FeCl_3.6H_2O$ in 100 mL deionized water. Similarly, ferrous solution was prepared by dissolution of 7.59g $FeCl_2.4H_2O$ in 100 mL deionized water. Both solutions were mixed in a beaker and heated upto 80 ℃ under continuous stirring. This was followed by the addition of 25 % NH_4OH in drops in order to increase the pH of $FeCl_3.6H_2O$ and $FeCl_2.4H_2O$ solution to 9.0 which is required for the formation of Fe_3O_4 photocatalyst. The resultant black precipitates were filtered, washed with deionized water severally and dried at 100 ℃ for 12 h. The overall chemical reaction is described as:

$$2FeCl_3 + FeCl_2 + 8NH_4OH \rightarrow Fe_3O_4 + 4H_2O + 8NH_4Cl \quad (1)$$

Chemical co-precipitation method was also adopted in preparation of $Zn@Fe_3O_4$ photocatalyst. For this purpose, 5 g of $ZnCl_2$ was disserved and added to the solution containing 17.59 g of $FeCl_3.6H_2O$ and 7.59g of $FeCl_2.4H_2O$ under constant stirring at a temperature of 80 ℃. Finally, 25 % NH_4OH solution was added slowly to the mixture of $FeCl_3.6H_2O$ and $FeCl_2.4H_2O$ to adjust the pH to 9.0 which is required for complete formation of $Zn@Fe_3O_4$. The brown precipitates formed were separated, washed with deionized water repeatedly and dried at 100 ℃ for 12 h (Fig.1).

Characterization of the photocatalysts

The crystallization properties of nano-Fe_3O_4 and $Zn@Fe_3O_4$ were analyzed by an X-ray diffraction (XRD, x port) with Cu Kα radiation (λ = 0.15406 nm, 30 kV, 30 mA). Morphological analysis of the photocatalysts was performed by using scanning electron microscopy (SEM) (JEOL ISM – 6390LV) at accelerating voltage of 10 kV and 500X magnification. The absorption spectra of the synthesized photocatalysts material were obtained by using UV-visible spectrophotometer (Drawell D8 Model). The absorption data was used to estimate the band gap energy by adopting the Schuster-Kubelka-Munk expression.

Photocatalytic degradation study

The photocatalytic performance of nano-Fe_3O_4 and $Zn@Fe_3O_4$ was studied by monitoring the degradation performance of the photocatalyst on methylene blue under ultra-violet light irradiation as reported elsewhere [12,19]. The catalysts (0.1g) were added into 100 mL solution containing 200 ppm MB. The mix suspension was stirred for 30 min in a dark environment to reach adsorption equilibrium. Afterward, the suspension was irradiated with ultraviolet light (254 nm, 220 V-15 w UV lamp) for 1hour intervals for upto 5 hours. The effect of photocatalyst dosage was studied at different weights of the photocatalysts (0.1 – 0.5 g). The photocatalytic efficiency was monitored with UV-Visible absorption spectrophotometer at 664 nm being maximum absorption wavelength of methylene blue. The percentage degradation of MB dye was calculated as follows:

$$\text{Percentage degradation} = \frac{A_0 - A_t}{A_0} \times 100 \quad (2)$$

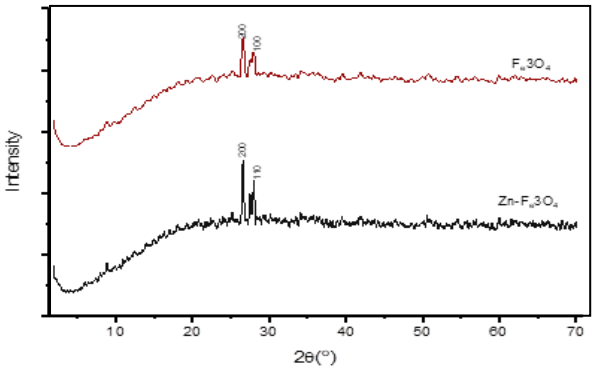

Fig. 2: XRD pattern of Fe_3O_4 and Zn@Fe_3O_4

Where A_o is dye absorbance at initial stage, A_t is dye absorbance at time t.

Computational study

In order to predict the site of interaction of the methylene blue atoms with the photocatalyst, the quantum chemical calculations of methylene blue were performed using DFT electronic program, DMol^3 using Generalized Gradient Approximation (GGA) and Becke exchange term with the Lee – Yang –Parr (BLYP) correlation functional by using as the basis in material studio 7.0 software (Accelrys USA). The quantum chemical approach was executed for determining the relationship between degradation efficiency and molecular properties of the dye and synthesized metal oxide. Different theoretical descriptors were calculated such as the Highest Occupied Molecular Orbital (HOMO), Lowest Unoccupied Molecular Orbital (LUMO) and other theoretical quantum descriptors using relevant equations.

RESULTS AND DISCUSSION

X-ray diffraction (XRD) analysis

The crystalline behavior of the synthesized nanoFe_3O_4 and Zn@Fe_3O_4 photocatalyst were examined with x-ray diffractometer. The XRD pattern of nano-Fe_3O_4 and Zn@Fe_3O_4 are displayed in Fig. 2. The XRD profile of Fe_3O_4 shows 2 peaks that corresponded to those of Fe_3O_4 cubic structure for space group Fdm3 which correlated to the standard JCPDS reference No. 19-0629 confirming the crystallinity of Fe_3O_4 at 2θ values of 26.58^0 and 28.02^0 corresponding to diffraction peaks from (200) and (100) planes respectively. The XRD profile of nano-Zn@Fe_3O_4 photocatalyst also exhibited crystal phase of nano- Fe_3O_4 cubic structure referenced in the standard JCPDS card No. 75-1610 file without any secondary phases as displayed in Fig. 2, which also shows 2 peaks at 2θ positions of 26.55° and 27.47° which can be assigned to diffraction (200) and (110) planes respectively [20]. The patterns of nano-Fe_3O_4 and Zn@Fe_3O_4 photocatalysts shows that no secondary phase was formed with Zn dopant into nano-Fe_3O_4 crystal lattice and no significant changes were observed in the XRD diffraction patterns of nano-Fe_3O_4 and Zn@Fe_3O_4 photocatalysts.

The mean crystalline size of nano-Fe_3O_4 and Zn@Fe_3O_4 photocatalyst were calculated using Debye-Scherer (Eq. (3)).

$$\text{Crystalline size} = \frac{K\lambda}{\beta\cos\theta} \quad (3)$$

Where K is a constant 0.891, λ is the wavelength of X-ray radiation (1.5406 nm), β is the Full Width at Half Maximum Intensity (FWHM) in radians and θ is diffraction angle at the position of peak maximum.

The average particle size of nano-Fe_3O_4 and Zn@Fe_3O_4 were estimated from the most intense peak (200) from the XRD data based on Debye-Scherrer formula [21,22]. However, the average particle size of Fe_3O_4 was 6.09 nm, which was smaller than nano-Zn@Fe_3O_4 (9.77 nm). From the obtained values, the mean crystalline size increases with introduction of zinc ions into the nano-Fe_3O_4 crystal lattice. The increase in the particle size observed in nano-Zn@Fe_3O_4 can be assigned to the difference in the ionic radius of the metal ions, as the ionic radius of Zn^{2+} (0.74 Å) is higher than that of Fe^{3+} (0.64 Å) and smaller than Fe^{2+} (0.76 Å). The increase in the particle size of the doped catalyst suggests that the presence of Zn^{2+} in the lattice structure may have existed in the form of zinc oxide, thereby increasing the grain growth in the structure which resulted in large particle size of nano-Zn@Fe_3O_4.

Optical properties analysis

Optical properties of nano-Fe_3O_4 and Zn@Fe_3O_4 were determined through UV- Visible absorption spectra, as a function of wavelength for the range of 200 to 800 nm as illustrated in Fig. 3. The maximum absorption peak of Fe_3O_4 was found to be 800 nm and Zn@Fe_3O_4 was observed at 750 nm. It was observed from the UV-Visible spectra, that the absorption peak decreases when doped with a zinc ion (Zn@Fe_3O_4). The decrease in absorbance may be attributed to some factors such as defects in grain structure, particle size and oxygen deficiency or formation of zinc oxide [23].

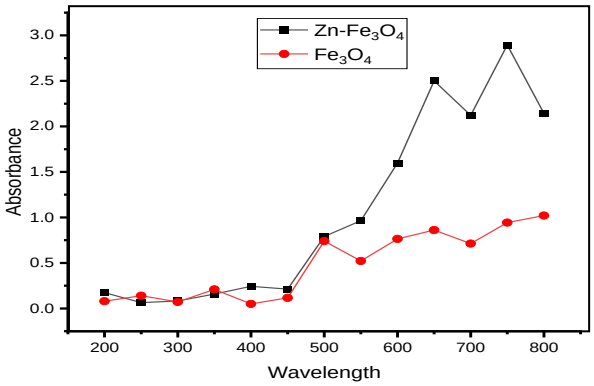

Fig. 3: Photo absorption spectra of Fe_3O_4 and $Zn@Fe_3O_4$

The band gap (E_g) of nanoFe_3O_4 and $ZnFe_3O_4$ were calculated using Kulbelka-Munk relation [24].

$$\alpha h\nu = C(h\nu - E_g)^n \quad (4)$$

Where α is absorption coefficient, h is plank's constant, ν is the frequency of light radiation, E_g is the band gap energy, C is a constant and "n" takes the value of $\frac{1}{2}$ for allowed direct transition. Plots of $(\alpha h\nu)^2$ against $(h\nu)$ are made for nano-Fe_3O_4 and $Zn@Fe_3O_4$ respectively. The band gap energy (E_g) was obtained from the most linear portions of the graphs on the x-axis. The band gap energy of Fe_3O_4 photocatalyst was found to be 2.77 eV and a slight shift was observed when it was doped with a zinc ion ($Zn@Fe_3O_4$) which increases to 2.80 eV as displayed in Fig. 4. The increase in the band gap indicates less ultraviolet light absorption by the doped photocatalyst. The increase in band gap energy (E_g) confirms the presence of Zn^{2+} in the Fe_3O_4 lattice. The increase in the band gap of the doped metal oxide may be attributed to the excessive presence of Zn ion in the matrix of the metal oxide or due to increase in the particle size as observed in the XRD result which might widen the band gap. The increase in band gap can also be attributed to the increase in the crystallite size and agglomerated nature of the doped metal oxide caused by the doping element. Despite the lack of an acceptable justification for the increase in the band gap of nano-$Zn@Fe_3O_4$ observed in this work, we suggest further investigation on the band gap of the zinc doped magnetic iron oxide.

Scanning electron microscopy (SEM) analysis

The SEM image of nano-Fe_3O_4 and $Zn@Fe_3O_4$ catalysts examined using scanning electron microscope are shown in Fig. 5. The SEM micrographs show that the surface of nano-$Zn@Fe_3O_4$ particles differs significantly from nano-Fe_3O_4. It can be seen that nano-Fe_3O_4 particles are dispersed and non-agglomerated in comparison with $Zn@Fe_3O_4$ particles that are in more agglomeration shape. The agglomeration of nano-$Zn@Fe_3O_4$ may be assigned to the presence of zinc ions that aggregated the particles. The observed grain sizes from the SEM micrographs reveal that the zinc doped nano-Fe_3O_4 may have a large particle size than Fe_3O_4 photocatalyst. *Emil-Kaya et al*. [4] have revealed that agglomerated particles do not show Photocatalytic activity.

Table 1: Elemental composition of Fe_3O_4 and $Zn@Fe_3O_4$ obtained from EDX analysis.

Elements (%)	Fe	O	Zn
Fe_3O_4	68.77	23.23	-
$Zn@Fe_3O_4$	47.22	25.45	27.33

EDX analysis

The percentage elemental composition of the synthesized nano-Fe_3O_4 and $Zn@Fe_3O_4$ were carried out and are tabulated in Table 1. It is evident that nano-$Zn@Fe_3O_4$ shows the presence of zinc in the zinc doped metal oxide nanoparticles. The result also shows a slight increase in the oxygen content in nano-$Zn@Fe_3O_4$ confirming the formation of metal oxides in the two synthesized nanoparticles.

Photocatalytic degradation

The photocatalytic activity of nano-Fe_3O_4 and $Zn@Fe_3O_4$ was evaluated using UV–Visible light assisted photodegradation of methylene blue by measuring the absorbance of the reaction mixture for the photodegradation process. The experiments were made under the effect of photocatalyst dosage and irradiation time.

Photocatalyst dosage

The effect of the amount of nano-Fe_3O_4 and $Zn@Fe_3O_4$ photocatalyst on the degradation of methylene blue dye was studied in range of 0.1-0.5 g and the result is displayed in Fig. 6a. An initial concentration of 200 mg/l of MB was used to study the effect of photocatalyst dosage. It was observed that, increase in the photocatalyst dosage increases the degradation rate of MB. The maximum degradation efficiency of MB obtained after treatment with nano-Fe_3O_4 and $Zn@Fe_3O_4$ for 60 mins at 0.5 g dosage was 83.8 % and 70.5 % respectively. The increase

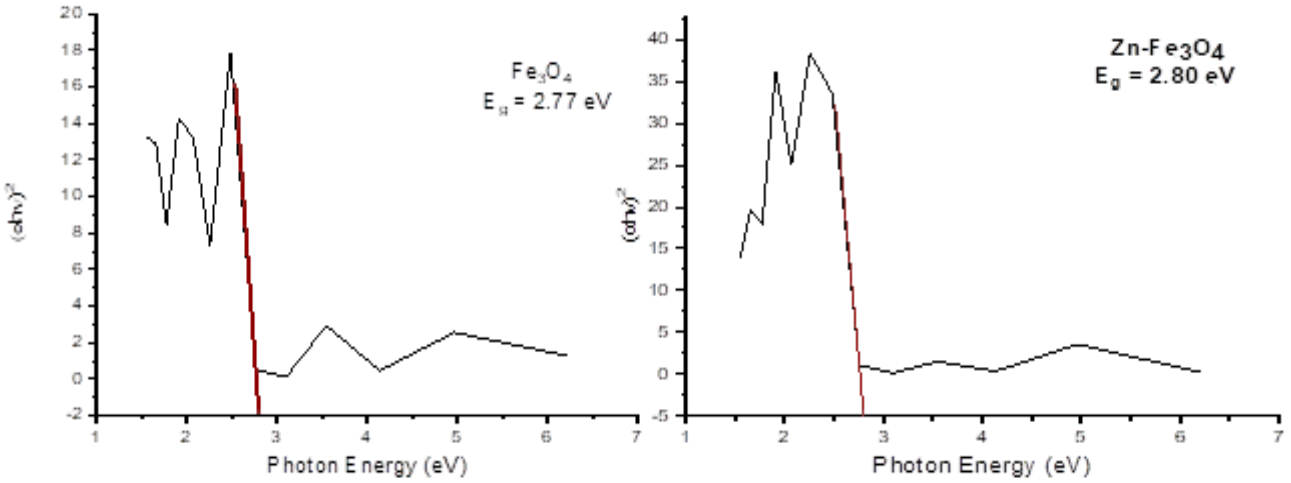

Fig. 4 Band gap spectra of synthesized Fe_3O_4 and $Zn@Fe_3O_4$

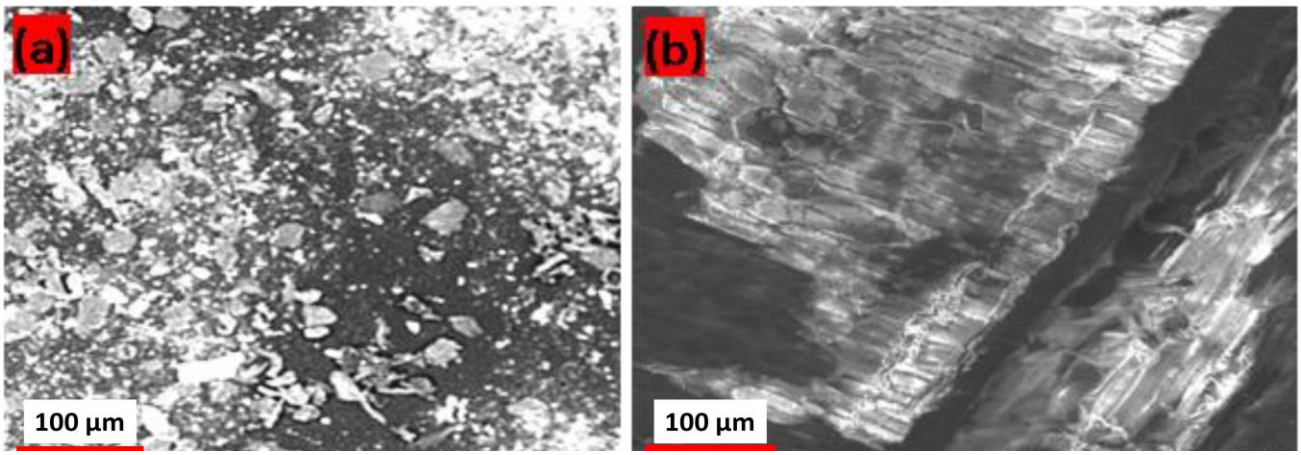

Fig. 5: Scanning electron micrographs of (a) Fe_3O_4 and (b) $Zn@Fe_3O_4$

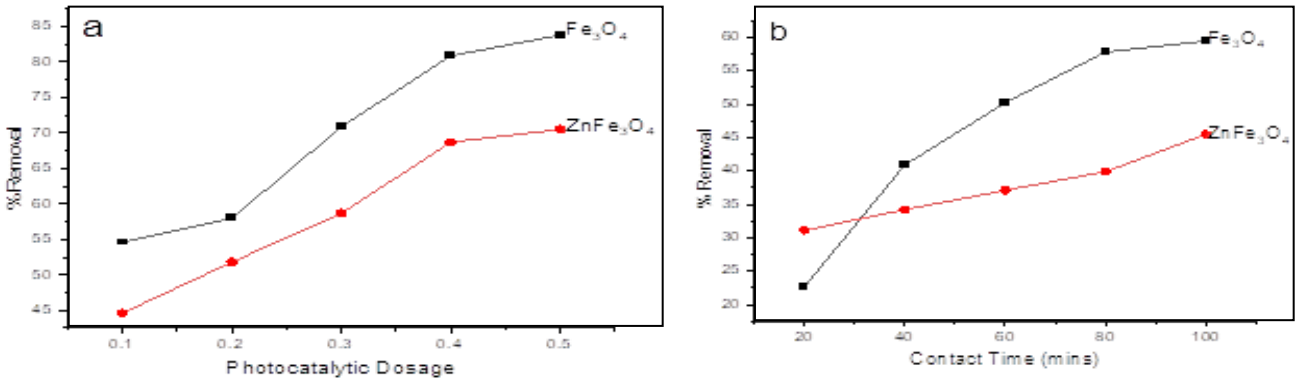

Fig. 6: Effect of (a) Photocatalyst dosage, (b) Contact time for catalytic activity

in the photocatalyst loading increases the photocatalytic degradation efficiency of MB. This phenomenon can be explained by the high amount of light absorbed due to increase in the number of active sites available on the photocatalyst surface [10] and due to increases in the level of hydroxyl and superoxide radicals generated [7,10]. The results obtained show optimum catalyst dosage at 0.4 g. However, no significant difference was observed at amount beyond the optimum catalyst loading. This may be assigned to the interception of light due increase in opacity

and light scattering by the metal oxide particles at high photocatalyst dosage leading to decrease in the passage of irradiation through the sample [10,24,25]. Furthermore, research has shown that increasing the photocatalyst dose above the optimum amount may also result in the agglomeration of particles in the lattice. Hence, these effects may cause some portion of the metal oxide surface becoming unavailable for photon absorption, thereby preventing illumination, generation a primary oxidant in the photocatalytic system ($^{\bullet}OH$) and reducing degradation efficiency respectively [26,27].

Effect of exposure time

The impact of exposure time was also investigated on the photocatalytic degradation of MB by varying the exposure time to UV light from 20 to 100 mins in the batch experiment. The comparison study on the degradation efficiency of dye under the nano-Fe_3O_4 and Zn@Fe_3O_4 showed varying results with increasing contact time as presented in Fig. 6b. The maximum removal percentage of MB degradation under initial concentration of 200mg, a photocatalyst dose of 0.2 g, contact time of 100 mins for nano-Fe_3O_4 and Zn@Fe_3O_4 were 59.4 % and 45.5 % respectively. The absorption of light with increase in exposure time explained the increase in the percentage degradation in the current result, because of increase in the promotion of electrons (e^-) from the valence band to the conduction band thus generating a hole in the valence band of the semiconductor catalyst [24]. Under favourable condition, electron and hole pairs of the conduction band and valence band travels towards the metal oxide surfaces which directly interacts with the dye solution, leading to oxidation and reduction reactions [28].

Effect of dopant on photocatalytic activity of photocatalyst

Metal doping plays a significant role on the photocatalytic performance of a metal oxide in the degradation of dye. Metallic doping of metal oxides may lead to the existence of intra-band levels that causes effective band gap contraction or expansion, which either improves or reduces its photocatalytic activity [10]. In this study, the introduction of zinc ion (Zn^{2+}) in Fe_3O_4 might have reduces the absorption of light in the ultraviolet region. This may be attributed to the increase in the band gap energy in nano-Zn@Fe_3O_4 particle. The low photocatalytic activity might also be caused by increase on the extent of undesired recombination of charge carrier, due to a poor overlap with light source spectrum [29]. Recent investigations have shown that the presence of dopant on the surface of metal oxide reduces its surface area, hinder the adsorption of reactant and thus, reduces its photocatalytic activity [24, 30]. High amount of dopant on the lattice of metal oxide may shield the metal oxide from the UV light and block the interfacial electron and hole transfer, thereby leading to low photo-activity [31]. The photocatalytic performance of doped photocatalyst can decrease the rate of dye degradation due to excessive surface oxygen vacancy and the nature of the dopant, which can become the recombination centers of photo-induced electrons and holes [32, 33]. This finding is in agreement with the results of *Bouras et al*. [34] on the photocatalytic degradation of basic blue 41 dye under UV light irradiation, which they reported good photocatalytic degradation in the presence of pure TiO_2, then in the presence of Fe doped TiO_2. This is a confirmation that transition metal doped metal oxide can also have negative effects on the photocatalytic degradation of some dyes [24].

The poor photocatalytic degradation of MB by nano-Zn@Fe_3O_4 observed in present work may be assigned to the increase in oxygen vacancy, high amount of metal dopant (Zn^{2+}) on the surface of nano-Fe_3O_4, poor crystallity of the doped metal oxide (Zn@Fe_3O_4), increase in particle size, and wide band gap. The poor enhancement of photodegradation for the doped metal oxide can also be attributed to the non-synergistic role of between the metal ions present in the doped metal oxide. This poor synergistic effect could be due to poor electronic interactions in the zinc doped magnetic iron oxide [35]. Akpan and Hameed [24] in their study offered explanation for the low photocatalytic activity of doped metal oxide. They suggested that when the dopant is in excess in the doped metal oxide, its existence reduces the specific area of the metal oxide, thereby impeding the adsorption of reactant and thus inhibits the photocatalytic activity.

In order to compare the performance of Fe_3O_4 and Zn@Fe_3O_4 nanoparticles, the maximum degradation rate of methylene blue obtained in this work was compared with several rescent work and the results are tabulated in Table 2. In comparison as shown in Table 2, the Zn@Fe_3O_4 nanoparticles had a poor performance in the degradation of MB in this study.

Table 2: Comparative potentials of various photocatalysts in the photodegradation of methylene blue.

Photocatalyst	Quantity (mg)	Removal efficiency (%)	Time (min)	Ref.
Fe_2O_3@MgO	0.1	91	120	[36]
Co-Fe_3O_4	25	92	120	[37]
Ag-PMOS	10	81	60	[38]
$CaPbFe_{12}O_{19}$ Composite	50	85	120	[39]
Yb2O3/GOCNNIONPs	5	83.5	45	[40]
Fe_3O_4/Zn@Fe_3O_4	50	83.8/70.5	60	this work

Mechanism of photocatalytic activity

The proposed mechanism occurring at the Fe_3O_4 and Zn@Fe_3O_4 photocatalyst surface causing the degradation of methylene blue dye is described by the following reactions (5) to (15) [34].

$$Fe_3O_4 + hv(UV) \rightarrow Fe_3O_4(h^+_{VB} + e^-_{CB}) \quad (5)$$

$$Fe_3O_4(h^+_{VB}) + H_2O \rightarrow Fe_3O_4 + H^+ + OH^- \quad (6)$$

$$Fe_3O_4(h^+_{VB}) + OH^- \rightarrow Fe_3O_4 + {}^{\bullet}OH \quad (7)$$

$$Fe_3O_4(e^-_{CB}) + O_2 \rightarrow Fe_3O_4 + {}^{\bullet}O_2^- \quad (8)$$

$${}^{\bullet}O_2^- + H^+ \rightarrow HO_2^{\bullet} \quad (9)$$

$$ZnFe_3O_4 + hv(UV) \rightarrow ZnFe_3O_4(h^+_{VB} + e^-_{CB}) \quad (10)$$

$$ZnFe_3O_4(h^+_{VB}) + H_2O \rightarrow ZnFe_3O_4 + H^+ + {}^{-}OH \quad (11)$$

$$ZnFe_3O_4(h^+_{VB}) + {}^{-}OH \rightarrow ZnFe_3O_4 + {}^{\bullet}OH \quad (12)$$

$$ZnFe_3O_4(e^-_{CB}) + O_2 \rightarrow ZnFe_3O_4 + {}^{\bullet}O_2^- \quad (13)$$

$${}^{\bullet}O_2^- + H^+ \rightarrow HO_2^{\bullet} \quad (14)$$

$$MB + {}^{\bullet}OH \rightarrow CO_2 + H_2O + \text{other degradation production} \quad (15)$$

Where *hυ* is absorbed photon energy necessary to excite the metal oxide electron from the Valence Band (VB) to Conduction Band (CB) region.

Computational modeling

In order to study the electron injection from dye to the photocatalyst and understand the molecular properties of methylene blue, Density Functional Theory (DFT) calculations were estimated with the aid of the Dmol^3 using GGA and BLYP as the basis set. The computational modeling was studied to understand the nature of MB interaction with the metal oxide surface. The quantum chemical descriptors such as dipole moment (μ), total energy (E_{total}), energy gap (ΔE), electronaffinity (A), electronegativity (χ), global hardness (η), ionization potential (I), global softness (σ) and global electrophilicity index (ω) were calculated using equation (16) to (22) [41].

Table 3: Quantum descriptors methylene blue studied

Descriptor	E_{HOMO} (eV)	E_{LUMO} (eV)	ΔE (eV)	η (eV)	σ (eV)	χ (eV)	ω	I (eV)	A (eV)
Values	-3.392	-1.346	2.045	1.023	0.978	2.369	2.743	3.392	1.346

$$\Delta E = E_{LUMO} - E_{HOMO} \quad (16)$$

$$\chi = -\frac{1}{2}(E_{LUMO} + E_{HOMO}) \quad (17)$$

$$\eta = -\frac{1}{2}(E_{LUMO} - E_{HOMO}) \quad (18)$$

$$\sigma = -\frac{1}{\eta} \quad (19)$$

$$\omega = \frac{\chi^2}{2\eta} \quad (20)$$

$$I = -E_{HOMO} \quad (21)$$

$$A = -E_{LUMO} \quad (22)$$

The optimized molecular structure and frontier molecular orbital of methylene blue are shown in Fig. 7. The optimized geometry structure, electron density, lowest unoccupied and highest occupied molecular orbital (LUMO and HOMO) of methylene blue is presented in Fig. 7 respectively. Consequently, electron density diagram as shown in Fig. 7 revealed that nitrogen is the major and favorite sites of interaction with the metal oxide surface. The quantum chemical descriptors of MB, in aqueous phase are grouped in Table 3.

Conversely, the HOMO energy (E_{HOMO}) shows high electron donating ability of the molecule. Molecules with high values of E_{HOMO} imply the capability to donate electrons to appropriate acceptor with low empty molecular orbital energy. The LUMO energy (E_{LUMO}) value indicates the electron accepting ability of the molecule; lower E_{LUMO} value shows higher ability of accepting electrons [30]. The eigenvalues of E_{HOMO} and E_{LUMO} orbital of the MB molecule were -3.392eV and -1.346eV respectively. The high value of E_{LUMO} demonstrates the ability of the MB dye in accepting electrons from the metal oxide photocatalyst. It can be observed that, the energy difference (2.045 eV) between the HOMO and LUMO is low which implies the ease with which electrons can be injected into conduction band of the dye. This indicates that, photocatalytic method in MB degradation because the low photon energy is required to inject an electron from the occupied orbital to unoccupied orbital [42,43].

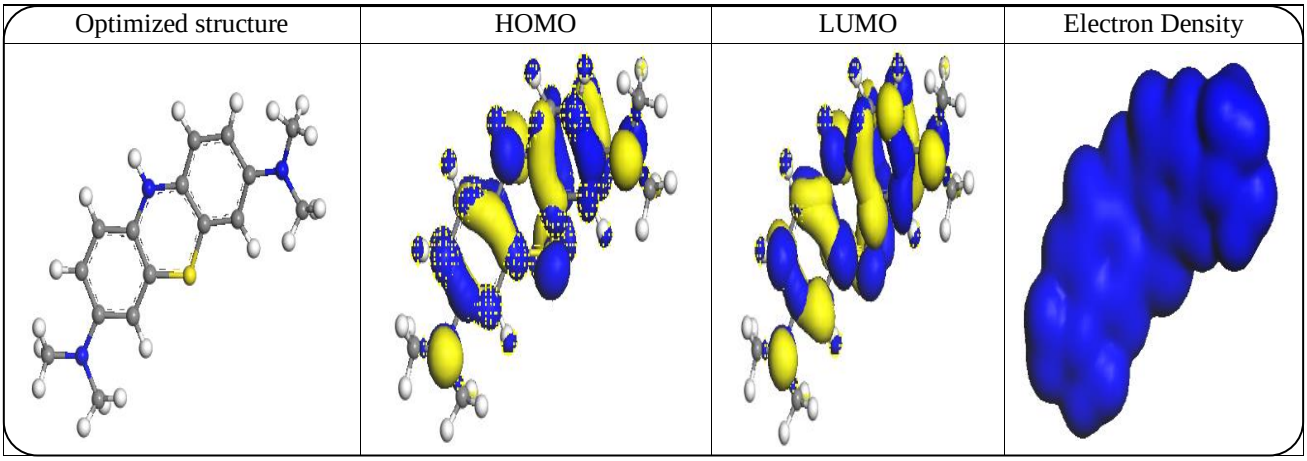

Fig. 7: Frontier molecular orbital, density and optimized structure of MB. Colour scheme: White = hydrogen, grey = carbon, blue = nitrogen, yellow = sulphur

CONCLUSION

Nano-Fe_3O_4 and Zn@Fe_3O_4 photocatalyst with reduced particle size were successfully synthesized by co-precipitation method and utilized in the photodegradation of methylene blue under ultraviolet light irradiation. The results obtained demonstrated good photocatalytic activity in degradation of methylene blue. Results showed that nano-Fe_3O_4 performed better in the degradation of MB than Zn@Fe_3O_4 catalyst under the same conditions. Scanning electron microscopy, x-ray diffraction and UV-Visible spectrophometry analysis validated the formation of synthesized metal oxide photocatalyst. Density Functional Theory (DFT) computational modeling shows the electrons and adsorption structures of MB dye. The poor photocatalytic activity observed with nano-Zn@Fe_3O_4 may be related to the increase in oxygen vacancy or high amount of zinc ion on the surface of nano-Fe_3O_4. The results of photocatalysis study shows that metal oxide and UV light irradiation have an influence on the photocatalytic degradation of methylene blue. The application of these photocatalyst has created needs for further studies.

Acknowledgements

The authors acknowledge the technical assistance of Apih Victory and Olelewe Evangel of Materials and Electrochemical Research Unit (MERU) of the Department of Chemistry/Biochemistry and Management of Federal Polytechnic Nekede, Owerri, Nigeria in making this study successful.

Received: Mar. 31, 2023; Accepted: Jun. 26, 2023

REFERENCES

[1] Nasiri A., Rajabi S., Hashemi M., $CoFe_2O_3$@ Methylcellulose/AC as a New, Green, and Ecofriendly Nano-Magnetic Adsorbent for Removal of Reactive Red 198 from Aqueous Solution, *Arabian Journal of Chemistry*, **15:** 1-19 (2020).

[2] Tamilisai R., Palanisamy P.N., Review on the Photocatalytic Degradation of Textile Dyes and Antibacterial Activities of Pure and Doped-ZnO, *Inter. J. Res. Inn. App. Sci.*, **2(8):** 15-19 (2018).

[3] Warsi M.F., Shaheen N. Sarwar M.I., Agboola P.O., Shakir I., Zuifiqar S., A Comparative Study on Photocatalytic Activities of Various Transition Metal Oxides Nanoparticles Synthesized by Wet Chemical Route, *Desal. Wat. Treat.*, **211:** 181-195 (2021).

[4] Emil-Kaya E., Evren B., Erdol Z., Ekinci D., Ipekoglu M., Ozenler S., Morphological, Microstructural and Photocatalytic Characterization of Undoped and Ni, Co Doped Fe_2O_3 Particles Synthesized by Sonochemical Method, *Turkish Journal of Chemistry*, **46:** 1897-1908 (2022).

[5] Blazeka D., Car J., Klobucar N., Juron A., Zavasnik J., Jagodar A., Kovacevic F., Krstulovic N., Photodegradation of Methylene Blue and Rhodamine B Using Laser-Synthesized ZnO Nanoparticles, *Materials*, **13:** 1-15 (2020).

[6] Asif M., Zafar M., Akhter P., Hussian M., Umer A., Razzaq A., Kim W-Y., Effect of Urea Addition on Anatase Phase Enrichment and Nitrogen Doping of TiO_2 for Photocatalytic Abatement of Methylene Blue, *Appl. Sci.*, **11:** 1-15 (2021).

[7] Gaikwad S., Jadhav N., Mahadik S., Thokal A.G., Mandake M.B., Review: Photocatalytic Degradation of Textile Azo Dyes, *International Journal of Advance Engineering and Research Development*, **4(4):** 88-91 (2017).

[8] Lau G.E., Abdulah C.A.C., Ahmed W.A.N.W., Assaw S., Zheng A.L.T, Eco-friendly Photocatalysts for Degradation of Dyes, *Catalysts*, **10:** 1-16 (2020).

[9] Afolabi H.K., Nasef M.M., Nordin N.A.H.M., Ting T.M., Haru N.Y., Saeed A.A.H., Isotherms, Kinetics, and Thermodynamics of Boron Adsorption on Fibrous Polymeric Chelator Containing Glycidol Moiety Optimized with Response Surface Method, *Arabian J. Chem.*, **14:** 103453 (2021).

[10] Gaya U.I., Sani K.I., Hamisu A., Synthesis of Visible Light Response S-SnO_2 Catalyst for Optimized Photodegradation of Bromophenol Blue, *Journal of Physical Chemistry and Functional Materials*, **4(2):** 22-33 (2021).

[11] Samadi M.H., Fallah S.A., Mahmoodi N.O., Preparation, Characterization, and Performance Study of PVDF Nanocomposite Contained Hybrid Nanostructure TiO2-POM Used as a Photocatalytic Membrane, *Iran. J. Chem. Chem. Eng. (IJCCE)*, **40(1):** 35-47 (2021).

[12] Ezeibe A.U., Nleonu E.C., Onyemenonu C.C., Arrousse N., Nzebunachi C.C., Photocatalytic Activity of Aluminium Oxide Nanoparticles on Degradation of Ciprofloxacin, *Saudi J. Eng. Technol.*, **7(3):** 132-136 (2022).

[13] Su F., Li P., Huang J., Gu M., Liu Z., Xu Y., Photocatalytic Degradation of Organic Dye and Tetracycline by Ternary Ag_2O/AgBr – CeO_2 Photocatalyst under Visible–light Irradiation, *Scientific Reports*, **11(85):** 1-13 (2021).

[14] Kamakshi T., Sundari G.S., Erothu H., Rao T.P., Synthesis and Characterization of Graphene-Based Iron Oxide (Fe_3O_4) Nanocomposites, *Rasayan J. Chem.*, **11(3):** 1113-1119 (2018).

[15] Amirmahani N., Mahdizadeh H., Malakootian M., Pardakhty A., Mahmoodi N.O., Evaluating nanoparticles Decorated on Fe_3O_4@SiO-Schiff Base (Fe_3O_4@SiO-APTMS-HBA) in Adsorption of Ciprofloxacin from Aqueous Environments, *Journal of Inorganic and Organometallic Polymers and Materials*, **30:** 3540-3551 (2020).

[16] Saeed M., Usman M., Muneer M., Akrom N., Ulhaq A., Tariq M., Akram F., Synthesis of Ag-Fe_3O_4 Nanoparticles for Degradation of Methylene Blue in Aqueous Medium, *Bull. Chem. Soc. Ethiop.*, **34(1):** 123-134 (2020).

[17] Razani A., Abdullah A.H., Fitrianto N.A.Y., Gaya U.I., Sol-Gel Synthesis of Fe_2O_3 -Doped TiO_2 for Optimized Photocatalytic Degradation of 2,4-Dichlorophenoxyacetic Acid, *Oriental Journal of Chemistry*, **33(4):** 1959-1968 (2017).

[18] Hafeez A., Beenish A., Ammara M., Investigation of Doping Effect on Structural, Optical, Antibacterial, and Toxicity Properties of Iron Doped Copper Oxide Nanostructure Prepared by Co-Precipitation Route, *Iran. J. Chem. Chem. Eng. (IJCCE)*, **41(3):** 777–786 (2022).

[19] Ezeibe A.U., Achilike J.J., Nleonu E.C., Atuegbu O.M., Photocatalytic Degradation of Ciprofloxacin Using Magnetic Iron Oxide, *Inter. J. Sci. Eng. Res.*, **10(6):** 1445-1448 (2019).

[20] Rayan D.A., Zayed M.A., Abd Al Maqsoud G.M., Structure, Optical, and Magnetic Properties of Magnetite Nanoparticles Doped with Zinc and Lanthanum and Prepared in Oxygen and Nitrogen Atmosphere, *Journal of Transition Metal Complexes*, **2:** 1–11 (2019).

[21] Abhinandan S., Dhiraj S., Sonochemically Synthesized Mesoporous Pyrophanite- $MnTiO_2$ Nanoparticles: Adsorbent for Removal of Commercial Malachite Green Dye, *Iranian J. Chem. Chem. Eng. (IJCCE)*, **41(8):** 2548-2560 (2022).

[22] Ibrahim M.M., Gaya U.I., Synthesis of Eosin Y-Sensitized Ag-TiO_2 Nano-Hybrid for Optimized Photocatalytic Degradation of Aqueous Caffeine. *J. Chil. Chem. Soc.*, **64(1):** 4275-4284 (2019).

[23] Roxy M.S., Ananthu A. Sumithranand V., Synthesis and Characterization of Undoped and Magnesium Doped Zinc Oxide Nanoparticles, *Int. J. Sci. Res. Sci. Eng. Technol.*, **8(2):** 134-139 (2021).

[24] Akpan U.C., Hameed B.H., Parameters Affecting the Photocatalytic Degradation of Dyes Using T_iO_2-Based Photocatalysts: A Review, *Journal of Hazardous Materials*, **170:** 520-529 (2009).

[25] Chakrabarti S., Dutta B.K., Photocatalytic Degradation of Model Textile Dyes in Wastewater using ZnO as Semiconductor Catalyst, *J. Hazard. Mater.*, **3112:** 269-278 (2004).

[26] Konstantinou I.K, Albanis T.A., T_iO_2 Assisted Photocatalytic Degradation of Azo Dyes in Aqueous Solution: Kinetic and Mechanistic Investigation. A Review, *Appl. Catal. B. Environ.*, **49:** 1-14 (2003).

[27] Huang M., Xu C., Wu Z., Huang Y., Lin J., Wu J., Photocatalytic Discolorization of Methyl Orange Solution by Pt Modified T_iO_2 Loaded on Natural Zeolite, *Dyes and Pigments*, **77:** 327-334 (2008).

[28] Abargues R., Navarro J., Rodriguez-Canto P.J., Maulu A., Sanchez-Royo J.F., Martinez-Pastor J.P., Enhancing the Photocatalytic Properties of PbS QD Solids: The Ligand Exchange Approach, *Nanoscale*, **11:** 1978-1987 (2019).

[29] Ramirez A.E., Montero–Mnuoz M., Lopez L.L., Ramos-Ibarra J.E., Coaquira J.A.H., Heinrichs B., Paez C.A., Significantly Enhancement of Sunlight Photocatalytic Performance of Zno by Doping with Transition Metal Oxides, *Sci. Reports*, **11:** 1-9 (2021).

[30] Liu G., Zhang X., Xu Y., Niu X., Zheng L., Ding X., The Preparation of Zn^{2+} - Doped T_iO_2 Nanoparticles by Sol-gel and Solid Phase Reaction Methods Respectively and Their Photocatalytic Activities, *Chemosphere*, **59:** 1367-1371 (2005).

[31] Li Y., Peng S., Jiang F., Lu G., Li S., Effect of Doping T_iO_2 with Alkaline – Earth Metal Ions on Its Photocatalytic Activity, *J. Serb. Chem. Soc*., **72(4):** 393-402 (2007).

[32] Gindose T.G., Review on the Removal of Organic Dyes by Photocatalytic Degradation Using Nanocomposite of Transitional Metal Oxides under Visible Light, *Int. J. Curr. Res.*, **11(11):** 8266-8276 (2019).

[33] Xin B., Wang P., Ding D., Liu J., Ren Z., Fu H., Effect of Surface Species on Cu-TiO_2 Photocatalytic Activity, *Appl. Surf. Sci*., **254:** 2589-2574 (2008).

[34] Bouras P., Stathatos E., Lianos P., Pure Versus Metal-Ion Doped Nanocrystalline Titania for Photocatalysis, *Appl. Catal. B: Environ.*, **73:** 51–59 (2007).

[35] Liaqat R., Mansoor M.A., Igbal I., Jilani A., Skakir S., Kalam A., Wageh S., Fabrication of Metal (Cu and Cr) Incorporated Nickel Oxide Films for Electrochemical Oxidation of Methanol, *Crystals*, **11:** 1-15 (2021).

[36] Venkatachalam A., Mark J.A.M., Deivatamil D., Revathi J., Prince Jesuraj J., Sunlight Active Photocatalytic Studies of Fe_2O_3 based Nanocomposites Developed via Two-Pot Synthesis Technique, *Inorg. Chem. Commun.*, **124:** 108417 (2021).

[37] Keerthana S., Yuvakkumar R., Ravi G., Kumar P., Elshikh M.S., Aikhamis H.H., Alrefaei A.F., Velauthapillai D., A Strategy to Enhance the Photocatalytic Efficiency of α-Fe_2O_3, *Chromosphere*, **270:** 129498 (2021).

[38] Shahzad K., Najam T., Bashir M.S., Nazir M.A., Rehman A.U., Bashir M.A., Shah S.S.A., Fabrication of Periodic Mesoporous Organo Silicate (PMOS) Composites of Ag and ZnO: Photocatalytic Degradation of Methylene Blue and Methyl Orange, *Inorg. Chem. Commun.*, **12:** 108357 (2021).

[39] Jamshaid M., Rehman A.U., Kumar O.P., Iqbal S., Nazir M.A., Anum A., Khan H.M., Design of Dielectric and Photocatalytic Properties of Dy-Ni Substituted $Ca_{0.5}Pb_{0.5}$-xFe_{12}-yO_{19} M-Type Hexaferrites, *J. Mater. Sci. Mater. Electron*., **32:** 16255-16268 (2021).

[40] Farooq N., Luque R., Hessien M.M., Qureshi A.M., Sahiba F., Nazir M.A., Rehman A.A., A Comparative Study of Cerium and Ytterbium- Based GO/g-C_3N_4/Fe_2O_3 Composites for Electrochemical and Photocatalytic Applications, *Appl. Sci.*, **11:** 1-15 (2021).

[41] Nleonu E.C., Haldhar R., Ubaka K.G., Onyemenonu C.C., Ezeibe A.U., Okeke P.I., Mong O.O., Ichou H., Arrousse N., Kim S.-C., Dagdag O., Ebenso E., Taleb M., Theoretical Study and Adsorption Behavior of Urea on Mild Steel in Automotive Gas Oil (AGO) Medium, *Lubricants*, **10(157):** 1-13 (2022).

[42] Ayuba A.M., Abubakar M., Computational Study for Molecular Properties of some of the Isolated Chemicals from Leaves Extract of *Guiera senegalensis* as Aluminium Corrosion Inhibitor, *Journal of Science and Technology*, **13(1):** 47-56 (2021).

[43] Verma D.K., Aslam R., Aslam J., Quraishi M.A., Ebenso E.E., Verma C., Computational Modeling: Theoretical Predictive Tools for Designing of Potential Organic Corrosion Inhibitors, *Journal of Molecular Structure*, **1236:** 1-21 (2021).